

Coronagraph focal-plane phase masks based on photonic crystal technology: recent progress and observational strategy

Naoshi Murakami ^{*a}, Jun Nishikawa ^b, Wesley A. Traub ^c, Dimitri Mawet ^d,
Dwight C. Moody ^c, Brian D. Kern ^c, John T. Trauger ^c, Eugene Serabyn ^c,
Shoki Hamaguchi ^e, Fumika Oshiyama ^e, Moritsugu Sakamoto ^e, Akitoshi Ise ^e,
Kazuhiko Oka ^a, Naoshi Baba ^a, Hiroshi Murakami ^f, Motohide Tamura ^b

^aDivision of Applied Physics, Faculty of Engineering, Hokkaido University, Sapporo, Hokkaido 060-8628, Japan;

^bNational Astronomical Observatory of Japan, 2-21-1 Osawa, Mitaka, Tokyo 181-8588, Japan;

^cJet Propulsion Laboratory, California Institute of Technology, 4800 Oak Grove Dr, Pasadena, CA 91109, USA;

^dEuropean Southern Observatory, Alonso de Cordova 3107, Vitacura, Santiago 763 0355, Chile;

^eDivision of Applied Physics, Graduate School of Engineering, Hokkaido University, Sapporo, Hokkaido 060-8628, Japan;

^fInstitute of Space and Astronautical Science, Japan Aerospace Exploration Agency (ISAS/JAXA), 3-1-1 Yoshinodai, Chuo-ku, Sagami-hara 252-0222, Japan

ABSTRACT

Photonic crystal, an artificial periodic nanostructure of refractive indices, is one of the attractive technologies for coronagraph focal-plane masks aiming at direct imaging and characterization of terrestrial extrasolar planets. We manufactured the eight-octant phase mask (8OPM) and the vector vortex mask (VVM) very precisely using the photonic crystal technology. Fully achromatic phase-mask coronagraphs can be realized by applying appropriate polarization filters to the masks. We carried out laboratory experiments of the polarization-filtered 8OPM coronagraph using the High-Contrast Imaging Testbed (HCIT), a state-of-the-art coronagraph simulator at the Jet Propulsion Laboratory (JPL). We report the experimental results of 10^{-8} -level contrast across several wavelengths over 10% bandwidth around 800nm. In addition, we present future prospects and observational strategy for the photonic-crystal mask coronagraphs combined with differential imaging techniques to reach higher contrast. We proposed to apply a polarization-differential imaging (PDI) technique to the VVM coronagraph, in which we built a two-channel coronagraph using polarizing beam splitters to avoid a loss of intensity due to the polarization filters. We also proposed to apply an angular-differential imaging (ADI) technique to the 8OPM coronagraph. The 8OPM/ADI mode avoids an intensity loss due to a phase transition of the mask and provides a full field of view around central stars. We present results of preliminary laboratory demonstrations of the PDI and ADI observational modes with the phase-mask coronagraphs.

Keywords: high-contrast imaging, extrasolar planets, photonic crystal, coronagraphy, eight-octant phase mask, vector vortex mask, polarization

1. INTRODUCTION

Direct imaging and characterization of extrasolar planets is one of the most attractive issues in modern astronomy. Recently, giant planets with several Jupiter masses have been directly imaged ¹⁻³. However, direct imaging of Earth-like planets is extremely challenging because of overwhelming intensity ratios (contrasts), such as 10^{-10} , between an Earth-like planet and its parent star. For solving this problem, high-contrast instruments are indispensable for strongly suppressing the bright star light.

*nmurakami@eng.hokudai.ac.jp; phone 81 11 706-6720; fax 81 706 706-7811

Focal-plane phase-mask coronagraphs are promising methods which theoretically realize perfect stellar elimination. Several kinds of coronagraph focal-plane masks have been proposed, for example, four-quadrant phase mask (4QPM)⁴, eight-octant phase mask (8OPM)⁵, optical or vector vortex masks (OVM or VVM)^{6,7}, and so on. The 4QPM and 8OPM divide a stellar image into four or eight sectors, and provide π phase difference between lights passing through the adjacent sectors. The OVM (or VVM) provides a helical phase structure $l_p \times \theta$, as a function of an azimuth angle θ (l_p is the so-called topological charge). It has been shown that $4N$ -segment phase masks or even-charged vortex masks can realize perfect stellar elimination^{7,8}. However, it is difficult to manufacture the focal-plane phase masks, because the masks have phase singular point at the center, and also because an achromatic phase modulation is very challenging.

In this paper, we report our recent activities for developing the phase mask coronagraphs based on the photonic crystal technology. We manufactured the photonic-crystal 8OPM and VVM, which have extremely small central singular points. The masks are placed between polarization filters for realizing an achromatic phase modulation utilizing a Pancharatnam-Berry's phase^{9,10}. We carried out laboratory demonstration of the 8OPM coronagraph using the JPL high contrast imaging testbed (HCIT). We also proposed to combine the phase mask coronagraphs with differential imaging techniques to enhance the achievable contrast. In the latter part of the paper, we report preliminary experimental results, acquired using a coronagraph simulator constructed at the laboratory in Hokkaido University, of the 8OPM coronagraph with an angular differential imaging (ADI) mode, and the VVM coronagraph with a polarization-differential imaging (PDI) mode.

2. PHOTONIC-CRYSTAL CORONAGRAPH MASKS

The photonic crystal is an artificial periodic nanostructure of refractive indices. The photonic crystal is an attractive device for the coronagraph focal-plane phase masks because of its extremely small manufacturing defect.

Figure 1 shows a cross-sectional view of the photonic-crystal coronagraph masks, manufactured by the Photonic Lattice Inc. A periodic corrugated structure is formed by means of electron-beam lithography on a substrate (synthetic fused silica) with a thickness of 1mm. Two dielectric materials, Nb_2O_5 and SiO_2 , are then deposited alternatively on the substrate by RF bias sputtering. The corrugated pattern formed on the substrate is preserved during the deposition of the two materials by the autocloning technique^{11,12}. We note that a thickness of the multilayer (about 130 layers) on the substrate is about 5 μm . The manufactured masks exhibit birefringent characteristics, and become half-wave plates (HWP) at designed wavelengths with space-variant fast and slow axes along the corrugated patterns.

When a centrally-focused, right-handed circularly polarized light enters to the space-variant HWP, the output light is converted to left-handed circularly polarized light. Then, the output light has an additional phase according to 2α (α is an orientation angle of the optical axis of the HWP). This additional phase is known as the Pancharatnam-Berry's phase^{9,10}. Thus the space-variant HWP enables to embed the space-variant arbitrary phase on the incoming circularly polarized light. For the specific case of $\alpha = \pm 45^\circ$, the HWP converts an incoming 0° linearly polarized light to that with an angle 90° , and embeds a π -phase difference between the lights passing through the HWP with $\alpha = 45^\circ$ and -45° . Thus the space-variant HWP is applicable both for the VVM and the 8OPM.

Figure 2 shows a picture and a scanning electron microscope (SEM) image of the manufactured photonic-crystal 8OPM. The directions of the stripes on the surface ($\alpha = \pm 45^\circ$) correspond to the fast axes of the space-variant HWP. As described above, this mask provides the π -phase difference between light beams passing through the adjacent octant regions. From the SEM image, we can see that manufacturing defect is extremely small, which have been roughly estimate to be about 400 nm for a central singular point and about 100 nm for an octant boundaries¹³.

In the fig. 2, we also show a magnified image of the manufactured VVM seen between two crossed polarizers. The radial fast axes, shown by arrows, embed a $2 \times 2\pi$ phase ramp on an incoming light. Thus this axially-symmetric HWP acts as an optical vortex mask with a topological charge of 2.

In general, a retardation of a wave plate depends on a wavelength, and thus it is difficult to realize an achromatic wave plate over a broad spectral range. For the focal-plane masks utilizing the Pancharatnam-Berry's phase, the coronagraph performance would severely degrade due to an error of the retardation. The polarization filtering will be a promising solution for broadening the operation spectral range of the coronagraph. For realizing the achromatic coronagraphs, it has been proposed to use crossed linear polarizers for the 8OPM^{5,13}, or circular polarizers for the VVM¹⁴, respectively.

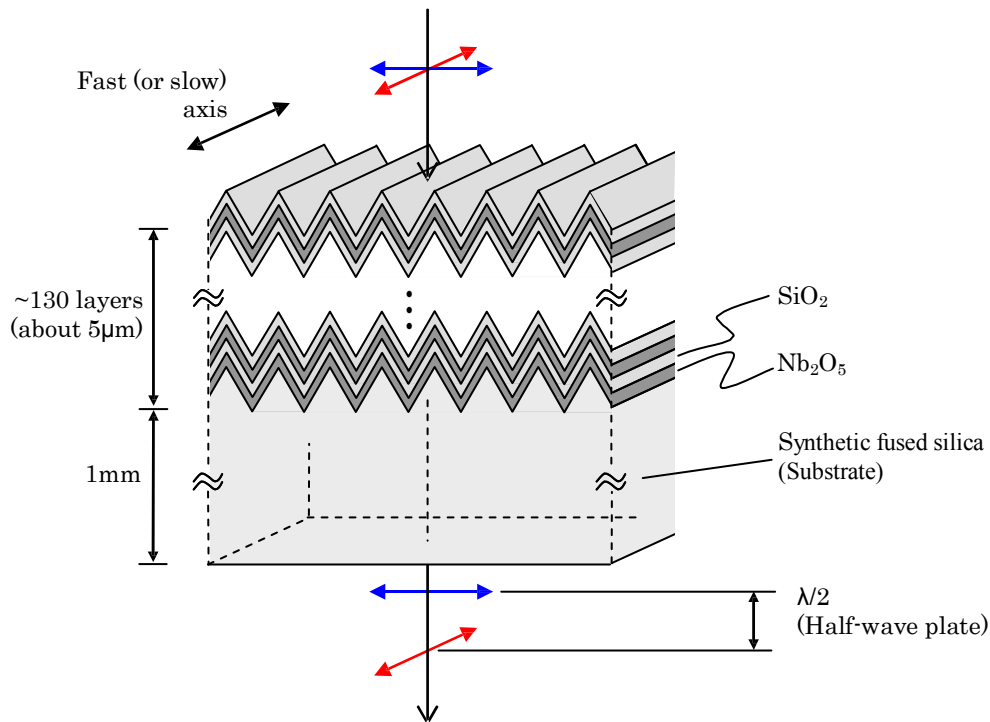


Figure 1. A cross-sectional view of a photonic-crystal phase mask based on the autocloning technique.

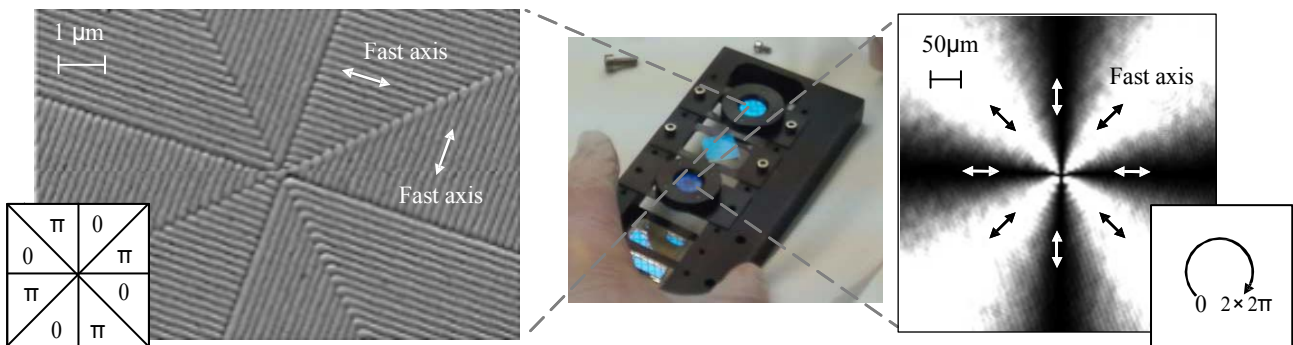


Figure 2. A picture and microscope images of an eight-octant phase mask (8OPM, left) and a vector vortex mask (VVM, right). The microscope image is taken by placing the VVM between two crossed polarizers.

3. LABORATORY DEMONSTRATION AT HCIT/JPL

3.1 The High-Contrast Imaging Testbed (HCIT)

We carried out laboratory demonstration of the 8OPM coronagraph on the high contrast imaging testbed (HCIT) at the Jet Propulsion Laboratory (JPL). The HCIT is a state-of-the-art coronagraph simulator installed into a vacuum chamber. Several kinds of coronagraphs have been tested at the HCIT/JPL¹⁵⁻²¹.

An optical configuration of the HCIT for the focal-plane coronagraph masks are shown in Fig. 2 of Ref. [21]. Several kinds of light sources are available, such as a monochromatic laser of $\lambda=785$ nm, or a supercontinuum light with selectable bandpass filters with bandwidths of 2%, 10%, and 20%. Light from a pinhole (a model star) is collimated by

an off-axis parabolic (OAP) mirror, and reflected on a Xinetics 32×32 deformable mirror (DM). An image of the model star is formed on a focal plane by a second OAP with a focal length of about 1500 mm. A polarizer (a diameter of $D=19.5$ mm) is placed between the DM and the second OAP for chromatic leakage filtering. The polarizer defines a size of an entrance pupil. Then, a physical scale of λ/D becomes about $62 \mu\text{m}$ on the focal plane where the photonic-crystal 8OPM is placed. Behind the 8OPM, the entrance pupil is reimaged by a third OAP with a magnification of about 0.52, and a Lyot stop (a diameter of 9 mm corresponding to 90% of the entrance pupil) is placed on the reimaged pupil. A second polarizer is placed behind the Lyot stop for the polarization filtering. The model star is imaged on a detector with a magnification of about 3 with respect to the first focal plane where the 8OPM is placed.

The DM is used to correct the wavefront error due to imperfection of the optical elements, and to create a “dark hole” against the residual speckle noise of the model star. The algorithm for the wavefront correction is called the electric field conjugation (EFC), because the DM actuators are controlled so as to create the negative of the electric field of the speckle noise²². The electric field created by the DM actuators is destructively interfered with the speckle noise on the detector. After the DM control, the electric field of the speckle noise is measured again, and then the wavefront is corrected iteratively to create a deeper dark hole.

A possible smallest inner working angle (IWA) is set to $2\lambda/D$ by the 8OPM itself. A possible largest outer working angle (OWA), on the other hand, is defined by the number of the DM actuators across the light beam (about 19 actuators resulting in the possible OWA of about $9\lambda/D$). In our experiments, we set the IWA and OWA for the EFC operation to $2.7\lambda/D$ and $7\lambda/D$, respectively.

3.2 Results of the laboratory demonstrations

In fig. 3, we show a result of the 8OPM coronagraph acquired using the supercontinuum light source with the 20% bandpass filter (a center wavelength of 800 nm and a bandwidth of 160 nm). We note that an effective bandwidth is smaller than 20% depending on a shape of the spectrum of the light source. A right graph shows a contrast profile along a horizontal line passing through a center of the dark hole (a white dashed line shown in the coronagraph image). We can see that a high contrast of about 2.4×10^{-8} can be achieved over the broad spectral range.

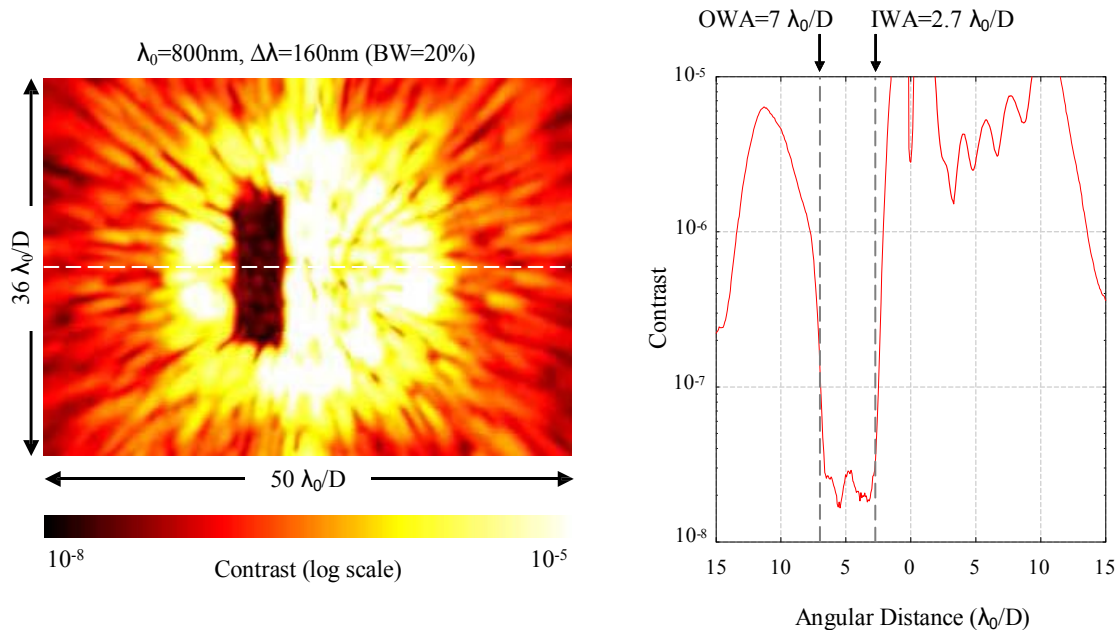


Figure 3. The 8OPM coronagraph image acquired with a broadband light source with a 20% bandpass filter (720-880nm). A dark hole is generated over a range between $2.7\lambda/D$ and $7\lambda/D$ from a suppressed model star. The left graph shows an intensity profile across a central horizontal line shown by a white dashed line in the image.

Figure 4 shows results of the 8OPM coronagraph acquired with the five 2% bandpass filters at five contiguous wavelengths around 800nm. Achieved contrasts over the dark holes are shown under the images and in a bottom graph. The best contrast could be obtained at $\lambda=800\text{nm}$, because the wavefront control is driven only at this wavelength. An average contrast over the 10% bandwidth covered by the five wavelengths is about 2.1×10^{-8} .

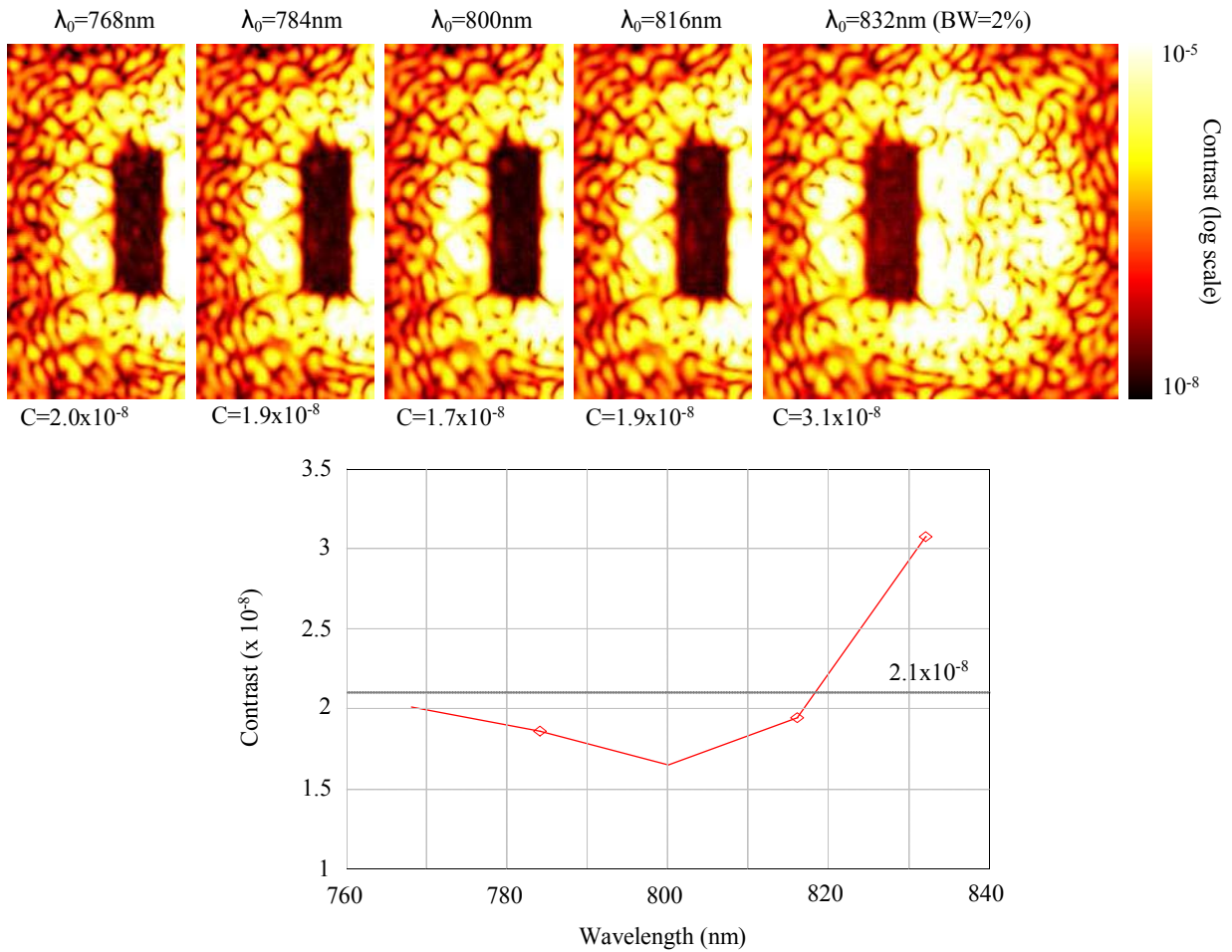


Figure 4. The 8OPM coronagraph images acquired with a five 2% bandpass filters. A bottom graph shows the achieved contrasts over the dark holes, as a function of the central wavelengths of the 2% bandpass filters.

4. COMBINATIONS WITH DIFFERENTIAL IMAGING TECHNIQUES

It is expected that combinations of the focal-plane phase-mask coronagraphs with differential imaging techniques will enhance the achievable contrast. We built a coronagraph simulator at the laboratory in Hokkaido University, and carried out laboratory demonstration of the angular differential imaging combined with the 8OPM coronagraph, and a polarization differential imaging (or a dual-channel imaging polarimetry) combined with the VVM coronagraph.

4.1 An angular differential imaging (ADI)

A drawback of the 8OPM coronagraph is an on-sky dead zone along the phase transitions of the mask, where planetary light is strongly reduced. However, this drawback can be avoided by combining the 8OPM coronagraph with the ADI technique²³. The ADI technique is a powerful tool for reducing a quasi-static speckle noise utilizing a field rotation

during tracking of targets by altitude/azimuth telescopes. The field rotation of the ADI observational mode is advantageous for the 8OPM coronagraph, because the planetary image moves across the dead zone as illustrated in an on-sky transmission map in fig. 5a.

We carried out laboratory demonstration of the 8OPM/ADI observational mode. A monochromatic He-Ne laser linked with a single-mode optical fiber is used for simulating a model star. Model planets are numerically added in the experimentally acquired coronagraphic images. A preliminary result of the 8OPM coronagraph without and with ADI is shown in fig. 5b and c, respectively. We set planet/star intensity ratios to 5×10^{-7} (“p1”) and 2.5×10^{-7} (“p2”), and star-planet angular separations to $5\lambda/D$. For the ADI mode, we acquired seven images with the field rotation from 0° to 240° with a 40° step. We can see that the image of the model planets, especially “p1”, can be clearly detected by the ADI.

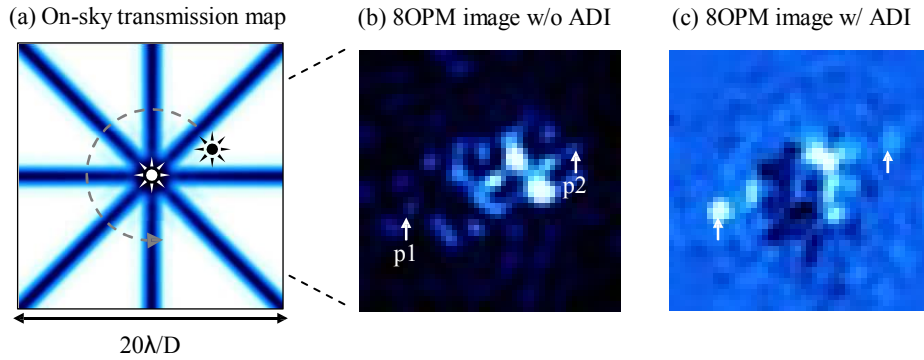


Figure 5. (a) On-sky transmission map of the 8OPM coronagraph. The map has a dead zone along phase transitions. The ADI mode rotates a field-of-view to avoid the dead zone. (b,c) Laboratory demonstration of the 8OPM coronagraph without and with the ADI mode, respectively. After the ADI, a model planetary image “p1” (a planet/star ratio of 5×10^{-7}) can be clearly detected, and “p2” (a planet/star ratio of 2.5×10^{-7}) is barely detected. Both model planets are located at $5 \lambda/D$ from a model star.

4.2 A dual-channel imaging polarimetry

A polarization differential imaging (PDI), or an imaging polarimetry, is also very attracting not only for reducing the residual speckle noise but also for characterizing planetary atmospheres and surfaces through polarization^{25,26}. Because the photonic-crystal coronagraph masks use the polarization filtering for achromatization, we can easily introduce the PDI observational mode by putting polarization modulator such as a rotating wave plate in front of the coronagraph optics.

A drawback of the polarization-filtered focal-plane coronagraph masks is an intensity loss due to the polarizing optics. By mitigating an effect of this drawback, a dual-channel coronagraphic configuration, based on polarizing beam splitters (PBS), has been proposed^{13,24}. When the dual-channel coronagraph is constructed, efficient high-contrast polarimetric observations can be realized by introducing a polarizing-beam splitter behind the coronagraph to observe coronagraph images of two orthogonally polarized components simultaneously. Figure 6a shows a schematic of the dual-channel coronagraph for the PDI observational mode. The polarization modulator in front of the coronagraph optics is then used for reducing non-common-path aberrations due to the dual-channel coronagraph.

We show a result of our preliminary laboratory demonstration of the dual-channel imaging polarimetry with the photonic crystal VVM. We used a He-Ne laser light for simulating unpolarized star light and partially polarized planetary light. The unpolarized star light and partially polarized planetary light (with a degree of polarization of about 45%) were simulated by 45° and 32° linearly polarized lights, respectively. We roughly set a planet/star intensity ratio to 1×10^{-4} and a star-planet angular separation to $5\lambda/D$.

As can be seen in fig. 6b, two coronagraph images of orthogonally polarized components are observed simultaneously on the same detector. The horizontal (X) and vertical (Y) polarized components can be switched between these two images by the polarization modulator. The modulation of polarized light enables to derive a polarimetric image (Stokes +Q and -Q images shown in Fig. 6c). We note that a difference between the Stokes +Q and -Q images can be calculated to derive the Stokes +2Q image for enhancing the planetary light (so-called double difference technique²⁷).

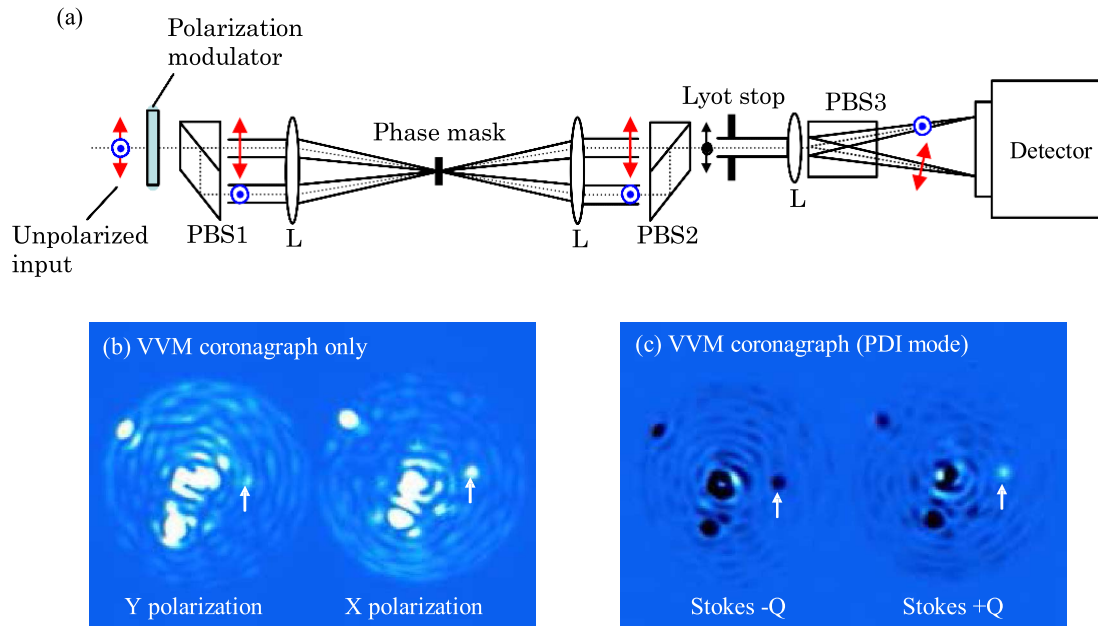


Figure 6. (a) A schematic of a fully-achromatic dual-channel coronagraph for the PDI observational mode. Bottom images show results of the laboratory demonstration of the VVM coronagraph (b) without and (c) with the polarimetric mode. Planetary images can be detected clearly as positive and negative spots (indicated by arrows), corresponding to of the Stokes +Q and -Q images, by using the polarimetric mode.

5. CONCLUSIONS

We manufactured the photonic crystal focal-plane coronagraph masks, 8OPM and VVM, based on the autocloning technique. The manufacturing defects of the photonic crystal masks are extremely small, which have been roughly estimate to be about 400 nm for a central singular point and about 100 nm for an octant boundaries. The manufactured masks are composed of wave plates with space-variant optic axes, which retardations are set to π (half-wave plate) at designed wavelengths. The masks provide phase modulations as a function of an orientation angle of the optic axes by the geometric or Pancharatnam-Berry's phase. Furthermore, the phase modulation can be achromatized by using the appropriate polarization filters.

We carried out laboratory demonstration of the 8OPM coronagraph at the HCIT/JPL, the state-of-the-art coronagraph simulator, in which the Xinetics 32×32 DM is incorporated for the wavefront correction. As a result, we attained average contrast of 2×10^{-8} across five wavelengths over 10% bandwidth around 800 nm.

We also proposed the photonic-crystal mask coronagraphs combined with differential imaging techniques to reach higher contrast. First, we proposed to apply an angular-differential imaging (ADI) technique to the 8OPM coronagraph. The ADI mode will be advantageous for the 8OPM and the other segment-type phase masks because it avoids an intensity loss due to a phase transition of the mask and provides a full field of view around central stars. Next, we also reported a dual-channel imaging polarimetric mode with the VVM coronagraph. In this observational mode, a two-channel coronagraph based on polarizing beam splitters is built to avoid a loss of intensity due to the polarization filters. We presented the results of the preliminary laboratory experiments of the both observational modes, and demonstrated that the residual speckle noise could be effectively reduced.

ACKNOWLEDGEMENTS

We acknowledge T. Kawashima of the Photonic Lattice Inc. for providing us with useful information on a photonic-crystal device. This work was carried out at the Hokkaido University, and at the Jet Propulsion Laboratory (JPL), California Institute of Technology, under a contract with the National Aeronautics and Space Administration (NASA). This research was supported by the National Astronomical Observatory of Japan (NAOJ), the Japan Aerospace Exploration Agency (JAXA) airborne and spacecraft instruments development program, and the Japan Society for the Promotion of Science (JSPS) through a Grant-in-Aid for Scientific Research(B) (19360036, 21340041), for JSPS Fellows (20-4783), and for Young Scientists(B) (23740139). This research was also partly supported by the Japanese Ministry of Education, Culture, Sports, Science, and Technology (MEXT), through a Grant-in-Aid for Scientific Research on Priority Areas, "Development of Extra-solar Planetary Science."

REFERENCES

- [1] Kalas, P., Graham, J. R., Chiang, E., Fitzgerald, M. P., Clampin, M., Kite, E. S., Stapelfeldt, K., Marois, C. and Krist, J., "Optical images of an exosolar planet 25 light-years from Earth," *Science*, 322, 1345-1348 (2008).
- [2] Marois, C., Macintosh, B., Barman, T., Zuckerman, B., Song, I., Patience, J., Lafrenière, D. and Doyon, R., "Direct imaging of multiple planets orbiting the star HR 8799," *Science*, 322, 1348-1352 (2008).
- [3] Lagrange, A.-M., Bonnefoy, M., Chauvin, G., Apai, D., Ehrenreich, D., Boccaletti, A., Gratadour, D., Rouan, D., Mouillet, D., Lacour, S. and Kasper, M., "A Giant Planet Imaged in the Disk of the Young Star β Pictoris," *Science* 329, 57- (2010).
- [4] Rouan, D., Riaud, P., Boccaletti, A., Clénet, Y. and Labeyrie, A., "The Four-Quadrant Phase-Mask Coronagraph. I. Principle," *Publ. Astron. Soc. Pacific*, 112, 1479-1486 (2000).
- [5] Murakami, N., Uemura, R., Baba, N., Nishikawa, J., Tamura, M., Hashimoto, N. and Abe, L., "An Eight-Octant Phase-Mask Coronagraph," *Publ. Astron. Soc. Pacific* 120, 1112-1118 (2008).
- [6] Foo, G., Palacios, D. M. and Swartzlander, Jr., G. A., "Optical vortex coronagraph," *Opt. Lett.* 30, 3308-3310 (2005).
- [7] Mawet, D., Riaud, P., Absil, O. and Surdej, J., "Annular Groove Phase Mask Coronagraph," *ApJ* 633, 1191-1200 (2005).
- [8] Carlotti, A., Ricort, G. and Aime, C., "Phase mask coronagraphy using a Mach-Zehnder interferometer," *A&A*, 504, 663-671 (2009).
- [9] Pancharatnam, S., "Generalized theory of interference, and its applications," *Proc. Indian Acad. Sci.* 44, 247-262 (1956).
- [10] Berry, M., "The adiabatic phase and Pancharatnam's phase for polarized light," *Journal of Modern Optics* 34, 1401-1407 (1987).
- [11] Kawakami, S., Kawashima, T. and Sato, T., "Mechanism of shape formation of three-dimensional periodic nanostructures by bias sputtering," *Applied Physics Letters* 74, 463-465 (1999).
- [12] Kawashima, T., Miura, K., Sato, T. and Kawakami, S., "Self-healing effects in the fabrication process of photonic crystals," *Applied Physics Letters* 77, 2613-2615 (2000).
- [13] Murakami, N., Nishikawa, J., Yokochi, K., Tamura, M., Baba, N. and Abe, L., "Achromatic eight-octant phase-mask coronagraph using photonic crystal," *ApJ* 714, 772-777 (2010).
- [14] Mawet, D., Serabyn, E., Liewer, K., Hanot, C., McElDowney, S., Shemo, D. and O'Brien, N., "Optical vectorial vortex coronagraphs using liquid crystal polymers: theory, manufacturing and laboratory demonstration," *Opt. Express* 17, 1902-1918 (2009).
- [15] Trauger, J. T. and Traub, W. A. "A laboratory demonstration of the capability to image an Earth-like extrasolar planet," *Nature* 446, 771-773 (2007).
- [16] Trauger, J., Moody, D., Gordon, B., Krist, J. and Mawet, D., "A hybrid Lyot coronagraph for the direct imaging and spectroscopy of exoplanet systems: recent results and prospects," *Proc. SPIE* 8151, 81510G (2011).
- [17] Belikov, R., Give'on, A., Kern, B., Cady, E., Carr, M., Shaklan, S., Balasubramanian, K., White, V., Echternach, P., Dickie, M., Trauger, J., Kuhnert, A. and Kasdin, N. J., "Demonstration of high contrast in 10% broadband light with the shaped pupil coronagraph," *Proc. SPIE*, 6693, 66930Y (2007).
- [18] Kern, B., Guyon, O., Give'on, A., Kuhnert, A. and Niessner, A., "Laboratory testing of a Phase-Induced Amplitude Apodization (PIAA) coronagraph," *Proc. SPIE*, 8151, 815104 (2011).

- [19] Mawet, D., Murakami, N., Delacroix, C., Serabyn, E., Absil, O., Baba, N., Baudrand, J., Boccaletti, A., Burruss, R., Chipman, R., Forsberg, P., Habraken, S., Hamaguchi, S., Hanot, C., Ise, A., Karlsson, M., Kern, B., Krist, J., Kuhnert, A., Levine, M., Liewer, K., McClain, S., McEldowney, S., Mennesson, B., Moody, D., Murakami, H., Niessner, A., Nishikawa, J., O'Brien, N., Oka, K., Park, P., Piron, P., Pueyo, L., Riaud, P., Sakamoto, M., Tamura, M., Trauger, J., Shemo, D., Surdej, J., Tabirian, N., Traub, W., Wallace, J. and Yokochi, K., "Taking the vector vortex coronagraph to the next level for ground- and space-based exoplanet imaging instruments: review of technology developments in the USA, Japan, and Europe," Proc. SPIE 8151, 815108 (2011).
- [20] Serabyn, E., Mawet, D., Wallace, J. K., Liewer, K., Trauger, J., Moody, D. and Kern, B., "Recent progress in vector vortex coronagraphy," Proc SPIE 8146, 81460L (2011).
- [21] Mawet, D., Serabyn, E., Moody, D., Kern, B., Niessner, A., Kuhnert, A., Shemo, D., Chipman, R., McClain, S. and Trauger, J., "Recent results of the second generation of vector vortex coronagraphs on the high-contrast imaging testbed at JPL," Proc. SPIE, 8151, 81511D (2011).
- [22] Give'on, A., Kern, B., Shaklan, S., Moody, D. C. and Pueyo, L., "Broadband wavefront correction algorithm for high-contrast imaging systems," Proc. SPIE, 6691, 66910A (2007).
- [23] Marois, C., Lafrenière, D., Doyon, R., Macintosh, B. and Nadeau, D., "Angular Differential Imaging: A Powerful High-Contrast Imaging Technique," ApJ, 641, 556-564. (2006)
- [24] Murakami, N., Inabe, T., Komatsu, T., Nishikawa, J., Hashimoto, N., Kurihara, M., Baba, N. and Tamura, M., "Polarization-interferometric eight-octant phase-mask coronagraph using ferroelectric liquid crystal for exoplanet detection," Proc. SPIE, 7731, 77314E (2010).
- [25] Kuhn, J. R., Potter, D. and Parise, B., "Imaging polarimetric observations of a new circumstellar disk system," ApJ, 553, L189-L191 (2001).
- [26] Baba, N. and Murakami, N., "A Method to Image Extrasolar Planets with Polarized Light," Publ. Astron. Soc. Pacific 115, 1363-1366 (2003).
- [27] Hinkley, S., Oppenheimer, B. R., Soummer, R., Brenner, D., Graham, J. R., Perrin, M. D., Sivaramakrishnan, A., Lloyd, J. P., Roberts, L. C., Jr. and Kuhn, J., "Speckle suppression through dual imaging polarimetry, and a ground-based image of the HR 4796A circumstellar disk," ApJ., 701, 804-810 (2009).